Analytical approach to the stochastic FitzHugh-Nagumo system and coherence resonance

B. Lindner and L. Schimansky-Geier
Institute of Physics, Humboldt-University at Berlin, Invalidenstrasse 110, D-10115 Berlin, Germany
(Received 1 June 1999; revised manuscript received 22 July 1999)

We consider the FitzHugh-Nagumo system under the influence of white Gaussian noise in the excitable regime. We present an analytical approximation in the limit of fast activator time scale. Marginal probability densities of a reduced system and dynamical quantities such as the pulse rate are found and the mean interspike interval and its relative standard deviation are investigated. The latter quantities allow a quantitative description of the phenomenon of coherence resonance, as comparisons with simulations show. [S1063-651X(99)04112-4]

PACS number(s): 87.19.La, 05.40.Ca

INTRODUCTION

The FitzHugh-Nagumo model (FHN) is a simplified variant of the famous Hodgkin-Huxley model accounting for the essentials of the regenerative firing mechanism in a excitable nerve cell [1,2]. From the mathematical point of view it is a simple example of an excitable deterministic dynamics and was the topic of many investigations in the past. Thereby, several versions of that model according to different physical situations display an interesting spectrum of deterministic dynamical effects with wide applicability in neuroscience, biology, and chemistry.

In reality, neurons are permanently affected by various sources of different kinds of noise, e.g., the fluctuative opening and closure of the ion channels within the membrane of the cell, noisy presynaptical currents and fluctuations of the distinct conductivities in the system, to name only a few. These fluctuations cause a sequence of stochastic excitations. The spike train and its properties have attracted much interest in recent studies on the constructive role of noise in nonlinear systems. For instance, if signals are input into the dynamics, stochastic resonance [3–6] as well as synchronization with the input signals [7,8] can be observed. Bursting behavior as in real neurons, e.g., occurs if additionally harmonic noise is implied in the system [9].

Similar to bistable dynamics, the application of stationary noise in excitable systems causes a new time scale, the mean excitation time of the occurrence of new spikes. Its value and the value of its variance depend significantly on the characteristics of the applied noise and hence noise controls both. On the other hand, the inherent recovery time of relaxing into the fixed point after firing does not really vary with the strength of the noise, whereas its variance grows with increasing noise.

Consequently, excitable systems driven by white noise exhibit the phenomenon of *coherence resonance* [10]. It occurs when the activation threshold is small with respect to the applied noise, whereas the noise impact on the variance of the excursion time is not yet relevant. In this case, which is clearly realized at a moderate noise intensity, the spike train exhibits an optimal regularity.

This effect has been studied numerically by different authors [10–12] and could recently be found experimentally in an excitable electronic circuit [13]. Also numerical simulations with coupled neurons were performed and the existence of optimally selected noise intensities and coupling coefficients were proven for a synchronously oscillating (ordered) response of the coupled network [14–16].

But, there is still a lack of analytical investigations of how, in the simplest case, additive white noise influences the dynamics of the FHN or, more generally, of excitable systems. Being generally a nonpotential system [17], even the analytical solution of the corresponding stationary Fokker-Planck equation is still a nontrivial task. A particular analytical solution was reported in [18] if assuming a special relationship between the parameters of the applied noise and those of the dynamics. The authors of [19] have proposed a perturbative approach to nonpotential systems in the bistable regime of a FHN.

Our analysis aims at the analytical determination of the stationary density as well as the stationary dynamical quantities in the excitable regime of the FHN. We consider the FHN in the limit of a fast voltage variable (activator) and with a noise source in the recovery variable (inhibitor). In this limit following a method by Melnikov [20], we find analytically the stationary marginal probability density of the nonpotential system and the rate of spikes in the voltage variable (pulse rate). As a result, we obtain the transfer function which reveals how the pulse rate is correlated with an adiabatically slow signal. Moreover, by calculating the first two moments of the mean passage times along the two slow branches of the FHN, we are able to find the mean time between pulses (in the literature also referred to as mean interspike interval) and its relative fluctuations and thus to provide analytical results concerning the coherence resonance in that system.

MODEL

With x being the so-called voltage variable and y the recovery variable, the dimensionless FHN dynamics is given by

$$\epsilon\dot{x} = x - x^3 - y + s,$$

$$\dot{y} = \gamma x - y + b + \sqrt{2D}\xi(t), \tag{1}$$

where ϵ is the time scale ratio of voltage and recovery variable. As a source of fluctuations, we include additive white noise in the equation of y. We introduce s standing for a

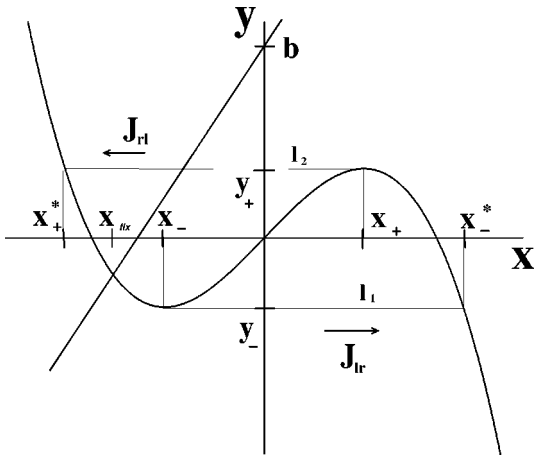

FIG. 1. Null clines of the system and some particular points used in the calculations. The system has one stable fixed point on the left branch of the cubic null cline. The currents J_{lr} and J_{rl} used in the approximation flow on the straight lines l_1 and l_2, respectively.

possible adiabatically slow signal. b and γ are parameters of the recovery determining the position of the fixed point as well as the typical duration of an excitation. Later on we set without loss of generality $s=0$. The sensitivity of the FHN with respect to adiabatically slow signals in the current can be expressed through the dependence on b. Transformation of the recovery variable $y \to y-s$ (neglecting time derivatives of s) leads to a modified $b \to b-s$.

The behavior of the system can be understood in terms of the null clines of the variables (cf. Fig. 1), i.e., the cubic function in x with maximum $P_{\max}=(x_+,y_+)$ and minimum $P_{\min}=(x_-,y_-)$ [21] and the straight line in y, respectively. The former consists of three distinct regions, separated by $P_{\max}, P_{\min}$: the stable left and right branches and the unstable middle branch. Choosing proper values of γ and b, both null clines intersect only once on the left stable branch (excitable regime), providing a single fixed point in $(x_{\rm fix}, y_{\rm fix})$. In the original work by FitzHugh [1], this point corresponds to the resting state of the nerve cell, while points at the right branch belong to the excited state and the points largely above the fixed point on the left-hand side belong to a refractory state.

We note that the voltage variable possesses a much smaller time scale than the recovery variable ($\epsilon \ll 1$ and $\epsilon \ll 1/\gamma$), i.e., the system is forced to relax fast to the x-null cline. Since the middle branch is unstable, the motion of the system is therefore restricted to a narrow region around the left and right branches and the two connecting lines between them.

The deterministic system ($D=0$) started at an appropriate initial state (for instance, with $y<y_-$) will make *one* long excursion in the phase space. First the trajectory reaches quickly the right branch, moving along this branch upwards until it reaches its top, and afterwards switching to the left branch, where it relaxes into the fixed point (which takes an infinite time). Then in the voltage variable one ''spike'' or ''pulse'' is observed.

With $D \neq 0$ and started in the fixed point, fluctuations allow the system after a typical activation time (the above-mentioned excitation time) to overcome the inherent threshold at (x_-,y_-) and—as in the deterministic case—to perform the excursion in the phase space returning back into the vicinity of the fixed point. In the course of time, therefore, a stochastic spike train of the voltage variable is generated (cf. Fig. 2). On one hand, in the stationary state this can be characterized by the pulse rate measured by time averaging,

$$r = \lim_{T\to\infty} \frac{N}{T}, \tag{2}$$

where N denotes the number of pulses during time T. On the other hand, the mean time between two pulses (mean interspike interval) may be considered,

$$\langle T \rangle = \lim_{N\to\infty} \frac{1}{N} \sum_{i=1}^{N} T_i ,$$

where T_i is the time between the ith and $(i+1)$th spike.

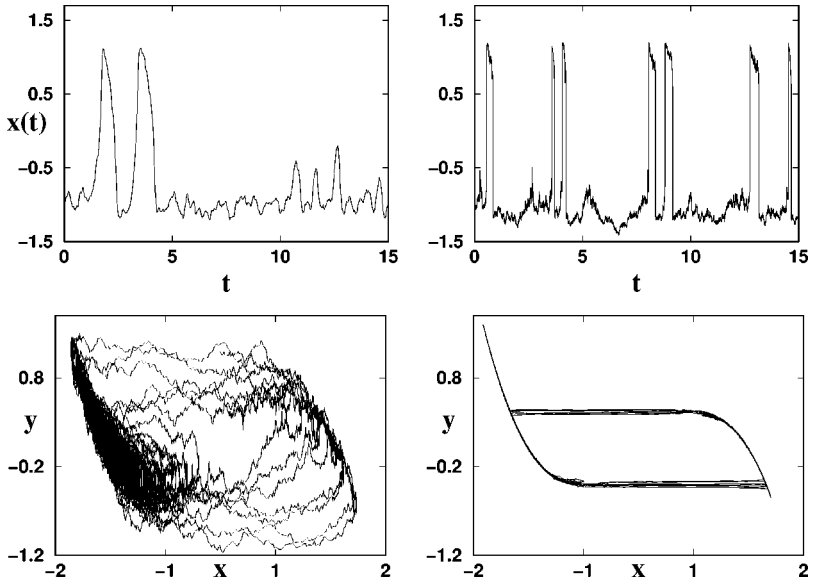

FIG. 2. Simulations of the stochastic differential equations. Voltage variable versus time and the corresponding trajectory in phase space for $\gamma=b=1.5, D=0.3$; left: $\epsilon=10^{-1}$, right: $\epsilon=10^{-4}$.

Both measures give the same information since in the long time limit when $\lim_{T\to\infty}$ is equivalent to $\lim_{N\to\infty}$,

$$r=\lim_{N\to\infty}\left(\frac{T_0}{N}+\frac{1}{N}\sum_{i=1}^{N}T_i+\frac{T_{N+1}}{N}\right)^{-1}=\frac{1}{\langle T\rangle}$$

holds, with T_0, T_{N+1} being the time intervals until the first or after the last spike, respectively.

As shown previously, possible adiabatically slow signals s would decrease additively the value of b. Therefore, the dependence of the rates on $-b$ can be thought of as a transfer function with respect to s. In [6] it was shown that the slope of the transfer function is proportional to the ''power norm'' introduced in [4]. This quantity measures the correlation of the output, i.e., the pulse rate of the FHN, to a sufficiently small signal s. Consequently, the sensitivity of the response to an adiabatically slow signal is characterized by the function

$$\frac{\partial r}{\partial s}=-\frac{\partial r}{\partial b}. \tag{3}$$

The pulse rate and the mean interspike interval does not characterize the regularity of the spike train. For that purpose, Pikovski *et al.* [10] introduced the standard deviation of the interspike interval as a *noise-to-signal ratio*,

$$R=\frac{\sqrt{\langle T^2\rangle-\langle T\rangle^2}}{\langle T\rangle}. \tag{4}$$

For Poissonian sequences with independent single excitations, R approaches unity. If $R<1$, the sequence becomes more regular and R vanishes for periodic deterministic excitations, for example in the deterministic limit cycle regime of Eq. (1). In the case $R<1$, excursions of the trajectories in the phase space can be interpreted as motion on a stochastic limit cycle [14,22].

We would like to mention that the occurrence of ordered sequences of excitations could be discussed also on behalf of spectral measures or correlation functions [22]. For our purpose, the quantity (4) is of advantage since it will require the first two moments of the interspike interval (ISI) distribution. Both moments will be available by the approach discussed below for arbitrary strength of the noise.

The system described by Eq. (1) is a ''nonpotential'' one, i.e., the corresponding Fokker-Planck equation (FPE) for the probability density $P(x,y)$,

$$\partial_t P=-\frac{1}{\epsilon}\partial_x(x-x^3-y)P+\partial_y(y-\gamma x-b+D\partial_y)P, \tag{5}$$

cannot be solved, even in the stationary case. Likewise not available are the marginal densities

$$\rho(x)=\int_{-\infty}^{+\infty}dy\,P(x,y),\quad p(y)=\int_{-\infty}^{+\infty}dx\,P(x,y),$$

which reveal how an ensemble of independent neurons is distributed over the excited and the resting state or the recovery variable, respectively.

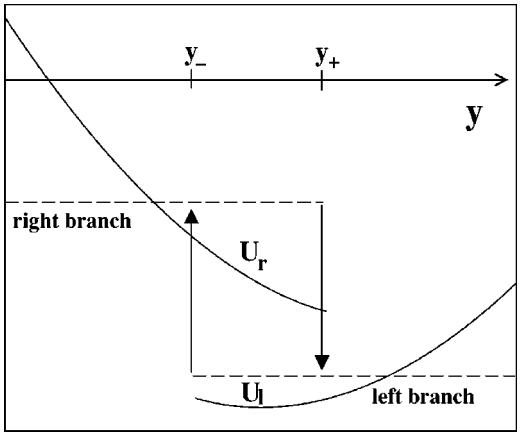

FIG. 3. Schematic picture of the system for $\epsilon\to 0$. Depicted are the effective potentials $U_l(y), U_r(y)$ (solid lines) for $\gamma=b=1.5$ and the absorption points y_+, y_-; the dashed lines indicate the two branches. Although the scheme resembles a Schmitt trigger, note that in this case the output depends on the slow variable y and is not a constant.

However, all these functions may be achieved by time averaging of a simulation of Eq. (1). We have used a simple Euler procedure with time step Δt, being two orders of magnitude smaller then ϵ (smallest time scale in the system), and we shall compare the analytical findings with numerical results.

With a look at the simulations at $\epsilon=10^{-4}$ in Fig. 2, one notes that the dynamics becomes effectively one dimensional in the limit $\epsilon\to 0$. In that case at least, $p(y), \rho(x), r, dr/db, T$, and R can be calculated analytically by solving two one-dimensional FPEs connected by appropriate boundary conditions and showing a constant flux through the system.

In this limit, the FHN system greatly resembles a Schmitt trigger (ST) driven by an Ornstein-Uhlenbeck process (OUP) [24,20]. The recovery variable y replaces the input variable of a Schmitt trigger. It is an OUP with correlation time equal to 1, intensity D, and centered around $\gamma x(t)+b$. Similarities and differences can be seen in Fig. 3. The dashed lines indicate two branches, i.e., the two basic states, namely resting and excited states, which are left at y_- and y_+, respectively. The slow variable y in each state is governed by respective effective potentials (see next section) drawn in the figure (solid lines).

On the other hand, there are several fundamental differences between the excitable system and a ST. First and most importantly, the excited state is governed by a dynamics without a fixed point. Its effective potential does not possess a minimum. As a result, the excited state is left even without the action of noise on the system. Contrary to the ST, no activation over a second barrier is necessary to return to the initial state. Second, the output is not a binary value, i.e., $x(y)$ depends itself strictly on the value of the slow variable. In addition, the dynamics at both branches are highly nonlinear.

PROBABILITY DENSITIES AND RATE

For small ϵ the voltage variable x relaxes fast toward one of the stable branches of the null cline $y=x-x^3$, where x

obeys the inverse of the cubic function on the left- or right-hand side, respectively [23],

$$x_l(y)=3y_-\cos\left(\frac{1}{3}\arccos(y/y_+)\right),$$
$$x_r(y)=3y_+\cos\left(\frac{1}{3}\arccos(y/y_-)\right). \tag{6}$$

In the limit $\epsilon\to 0$, the motion is restricted to these both lines. The two-dimensional Markovian system *separates into two one-dimensional subsystems* exchanging probability by currents J_{lr},J_{rl} infinitely fast via the straight lines l_1,l_2. In this limit there is no finite probability on these lines. Thus we obtain two coupled FPEs as was introduced for the first time by Melnikov [20], who considered the stochastic Schmitt trigger.

The FPEs of the two systems not only contain the usual drift and diffusion terms, but additional sources and sinks of probability, changing the probabilities at y_+ or y_-, respectively. They read

$$\partial_t P_l(y)=\partial_y[y-b-\gamma x_l(y)+D\partial_y]P_l+J_{rl}\delta(y-y_+),$$
$$\partial_t P_r(y)=\partial_y[y-b-\gamma x_r(y)+D\partial_y]P_r+J_{lr}\delta(y-y_-), \tag{7}$$

and $P_{\min}$ and $P_{\max}$ become now absorbing boundaries for the left and right branch, respectively. This implies

$$J_{lr}=D\partial_y P_l(y)_{y=y_-},\quad J_{rl}=-D\partial_y P_r(y)_{y=y_+}, \tag{8}$$

while in $y\to\pm\infty$ the densities obey natural boundary conditions on the respective branches. Furthermore, the sum of probabilities on both sides is conserved,

$$\int_{y_-}^{\infty}P_l(y)dy+\int_{-\infty}^{y_+}P_r(y)dy=1. \tag{9}$$

In steady state the currents have to be constant and coincide with each other and to the pulse rate introduced in Eq. (2),

$$J_{lr}=J_{rl}=r. \tag{10}$$

With Eqs. (9) and (10), one finds the solutions of the coupled FPEs (7),

$$P_l(y)=\frac{r}{D}e^{-U_l(y)/D}\int_{y_-}^{y}dz\,e^{U_l(z)/D}\Theta(y_+-z), \tag{11}$$

$$P_r(y)=\frac{r}{D}e^{-U_r(y)/D}\int_{y}^{y_+}dz\,e^{U_r(z)/D}\Theta(z-y_-), \tag{12}$$

with the effective potentials $U_l(y),U_r(y)$ explicitly given by

$$U_l(y)=\frac{(y-b)^2}{2}-\gamma\frac{x_l(y)}{4}[3y-x_l(y)],$$
$$U_r(y)=\frac{(y-b)^2}{2}-\gamma\frac{x_r(y)}{4}[3y-x_r(y)]. \tag{13}$$

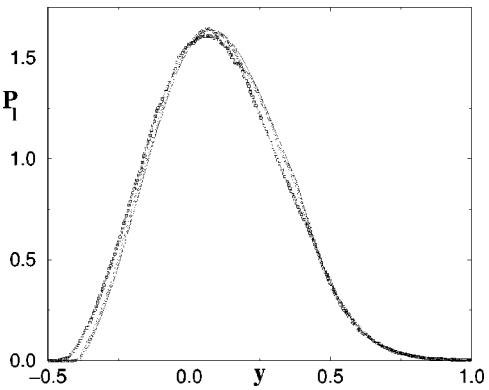

FIG. 4. The probability density on the left branch. The approximation (solid lines) is compared to simulations of the Langevin equations (squares and circles), which give by time averaging the shown marginal densities. Parameters are $D=0.1,\gamma=1.5,b=1.5,\epsilon=10^{-3}$ (squares), and $\epsilon=10^{-5}$ (circles).

$U_l(y)$ has a minimum at the fixed point, while the maximum of the densities depends on the pulse rate, which is obtained by Eq. (9) as

$$r=D\left[\int_{y_-}^{y_+}du\int_{u}^{\infty}dv e^{[U_l(u)-U_l(v)]/D}+\int_{y_-}^{y_+}du\int_{-\infty}^{u}dv e^{[U_r(u)-U_r(v)]/D}\right]^{-1}. \tag{14}$$

A. Probability densities

The rate is always positive. Therefore, it can be shown that *the maximum of the density* $P_l(y)$ occurs above the position of the fixed point, as can be seen for a particular set of parameter in Fig. 4. On the other hand, there exists at least one maximum on the right branch (Fig. 5), which can never be outside $[y_-,y_+]$. The total probability on this branch is comparably small (note the different scale in Fig. 5). The comparison to the simulations reveals a satisfactory agreement for $\epsilon=10^{-5}$, while for a larger value the assumed absorbing boundary condition fails significantly and the total probability on the right-hand side declines.

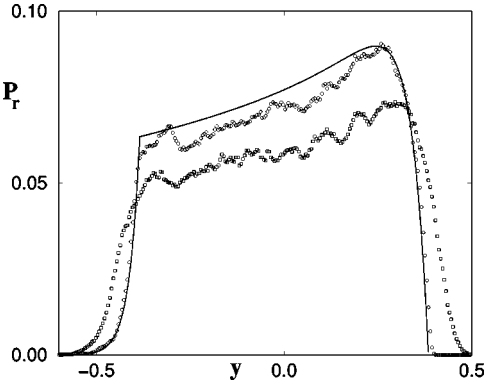

FIG. 5. The probability density on the right branch. The approximation (solid lines) is compared to simulations of the Langevin equations (squares and circles), which give by time averaging the shown marginal densities. Parameters as in Fig. 4.

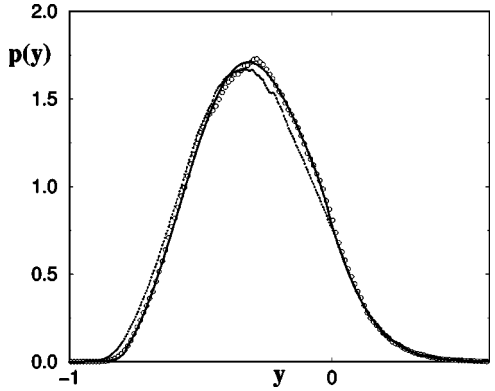

FIG. 6. Density $p(y)$, simulations at different values of ϵ compared to approximation (parameters as above).

The marginal density $p(y)$ is readily obtained by summation of P_l and P_r and is depicted in Fig. 6. The main contribution to that density comes from the left branch, therefore $p(y)$ looks similar to $P_l(y)$.

Taking into account the change of the volume element, the marginal density $\rho(x)$ is given by $\rho(x)=p(y)|dy/dx|$. It does not exhibit any contribution between $x_{\min}$ and $x_{\max}$, since, as supposed in our approach, there is no probability on the straight lines between the branches. In contrast, simulations at finite ϵ provide a small amount of probability within that range, which becomes comparably small by a decrease of ϵ in the *logarithmic* plot Fig. 7. The density around the maxima agrees fairly well with the numerical data.

B. Pulse rate

The pulse rate (14) can be evaluated numerically and results are presented in Figs. 8, 9, and 10. We first note that our formula (14) is clearly an overestimation of the rate at finite ϵ for two reasons: first, the motion between the branches obviously takes a finite time. Second, a finite ϵ causes subthreshold oscillations, diminishing the rate as well. Nevertheless, the approximation confirms quantitatively the simulations at sufficiently small ϵ, apart from the case of large γ, to which we shall return below.

Estimations can be made for small and large noise intensities. For small D, Eq. (14) may be simplified to [25]

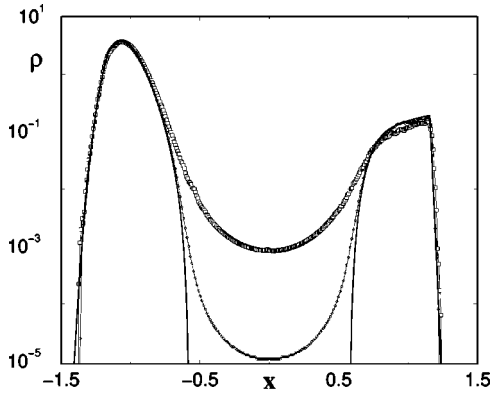

FIG. 7. Log plot of $\rho(x)$, simulations at different values of ϵ compared to approximation. Parameters as above.

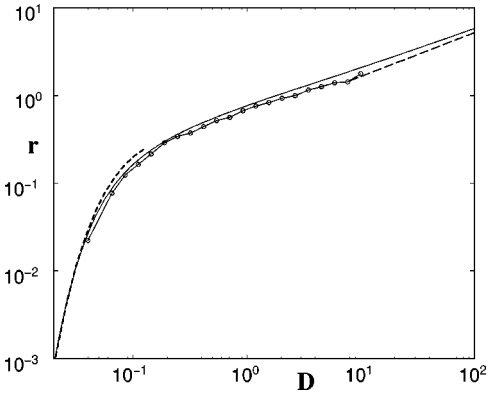

FIG. 8. Pulse rate versus noise level D, with $\gamma=0.8, b=0.9, \epsilon=10^{-4}$. Approximation Eq. (14) (solid line) compared to simulations (circles) and to the simplified expressions (15) (dashed) and (16) (long dashed).

$$r \approx U_l''(y_{\rm fix}) \sqrt{\frac{\Delta U_l}{\pi D}} e^{-\Delta U_l/D}, \quad D \ll \Delta U_l \tag{15}$$

with $\Delta U_l = U_l(y_-) - U_l(y_{\rm fix})$ being the potential barrier between the fixed point and the absorbing boundary. For large D, one finds the rate obeying

$$r \approx \frac{\sqrt{2D}}{4y_+\sqrt{\pi}}, \quad D \gg \Delta U_l . \tag{16}$$

In general, a monotonous behavior is obtained by an increase of the noise strength (Fig. 8). Trajectories reach more often the absorbing boundaries and the rate increases with growing noise. The simulation is compared to the expressions (15) and (16) for small and large D too and shows the validity of those formulas.

The impact of the slope γ is illustrated in Fig. 9, where we have chosen $b=y_{\rm fix}-\gamma x_{\rm fix}$. The fixed point remains at the same position; an increase of γ turns the null cline of y in a positive sense. Doing so, the excursion time is reduced yielding an increase of the rate for small γ. At the same time the effective barrier [see Eq. (13)] is enlarged, decreasing the rate for large γ. Thus, a maximum of the rate with respect to

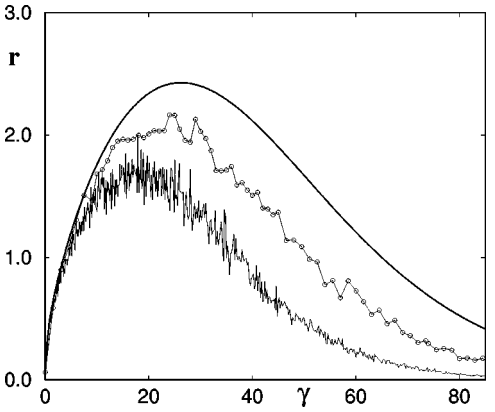

FIG. 9. Pulse rate versus the slope γ, while $D=0.1$ and the fixed point is fixed to $x_{\rm fix}=-0.8$, therefore $b=b(\gamma)$. Approximation Eq. (14) (solid line) compared to simulations with $\epsilon=10^{-4}$ (thin solid line) and $\epsilon=10^{-5}$ (circles).

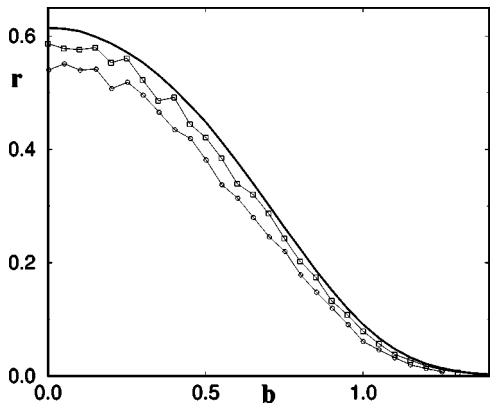

FIG. 10. Pulse rate versus b for $D=0.05, \gamma=1.0$. Approximation Eq. (14) (solid line) compared to simulations with $\epsilon=10^{-3}$ (circles) and $\epsilon=10^{-4}$ (squares).

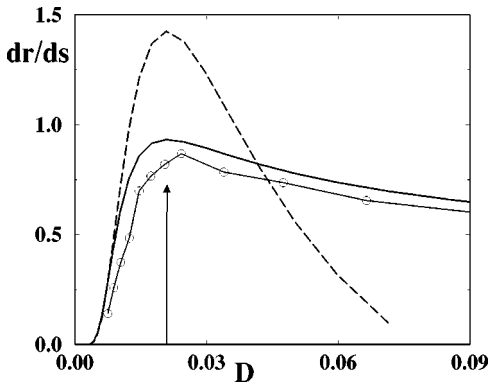

FIG. 11. The derivative of pulse rate with respect to s versus noise strength D for $b=0.7, \gamma=1.0$. Approximation Eq. (17) (solid line) and simplified expression Eq. (18) (dashed line) compared to simulations with $\epsilon=10^{-3}$ (circles). The arrow indicates the maximum calculated by Eq. (19).

γ is observed in Fig. 9, indicating an optimal value of the rate in the model (1). Note that for growing γ, the deviation of the predicted rate from the simulation data becomes stronger since the assumed time scale separation between the activator and inhibitor variable is weakened.

Variation of parameter b changes the position of the fixed point; an increase of it enlarges the distance to the threshold and diminishes therefore monotonously the rate (Fig. 10).

C. Sensitivity to adiabatically slow signals

As outlined previously, an important quantity is the derivative of the pulse rate with respect to a possible additive signal s in the activator dynamics. It is found by

$$\frac{\partial r}{\partial s}=-\frac{\partial r}{\partial b}=\frac{\int_{y_-}^{y_+}du\left(\int_u^\infty dv(v-u)e^{[U_l(u)-U_l(v)]/D}+\int_{-\infty}^{u}dv(v-u)e^{[U_r(u)-U_r(v)]/D}\right)}{\left[\int_{y_-}^{y_+}du\left(\int_u^\infty dve^{[U_l(u)-U_l(v)]/D}+\int_{-\infty}^{u}dve^{[U_r(u)-U_r(v)]/D}\right)\right]^2}. \tag{17}$$

A simplified expression is obtained by derivating Eq. (15), where we neglect the b dependence of the curvature $U_l''(y_{\rm fix})$. It yields

$$\frac{\partial r}{\partial s}\approx\frac{U_l''(y_{\rm fix})(y_{\rm fix}-y_-)}{\sqrt{\pi D\Delta U_l}}\left(\frac{\Delta U_l}{D}-\frac{1}{2}\right)e^{-\Delta U_l/D},\quad D\ll\Delta U_l. \tag{18}$$

The interesting fact is that the function $\partial r/\partial s$ displays a maximum with regard to the noise strength at a moderate value. From Eq. (18) the maximal slope is found to appear at

$$D_{\rm max}\approx 2(2-\sqrt{3})\Delta U_l. \tag{19}$$

As numerically demonstrated in [6], a nonmonotonous behavior with respect to D is a fingerprint of *aperiodic stochastic resonance*. The slope is in linear approximation proportional to the ''power norm,'' i.e., the cross correlation between an adiabatically slow signal $s(t)$ and the output firing rate. The value of the noise $D_{\rm max}$ where the maximum occurs can be estimated by Eq. (19) and is indicated in Fig. 11 by an arrow. Note that the curve being the result of simulations at a fairly large voltage time scale ($\epsilon=10^{-3}$) is always below the analytical curve (solid line) and the maximum occurs at a slightly larger noise intensity. As for the previous results, however, the convergence of simulations and theory can be improved by decreasing ϵ (not shown in the figure). We would like to point out the similarity of our analytical result with Fig. 7(c) in [6].

NOISE-TO-SIGNAL RATIO

The mean time between two spikes, i.e., the mean interspike interval, is given by the sum of the passage times from the injection to the absorption point on each branch. Therefore, in estimating the time sequence of the spikes, one deals with the classical mean first passage time (MFPT) problem and can use standard formulas [26].

The first and second moments on both branches are statistically independent and obey

$$\langle T_l(y_+)\rangle=\frac{1}{D}\int_{y_-}^{y_+}due^{U_l(u)/D}\int_u^\infty dve^{-U_l(v)/D}, \tag{20}$$

$$\langle T_l^2\rangle=\frac{2}{D}\int_{y_-}^{y_+}due^{U_l(u)/D}\int_u^\infty dve^{-U_l(v)/D}\langle T_l(v)\rangle, \tag{21}$$

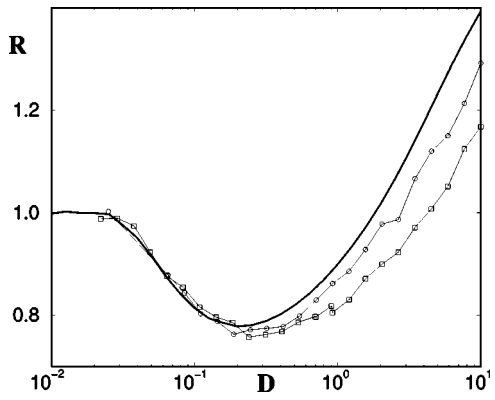

FIG. 12. Relative fluctuations versus noise strength D, with $\gamma = 0.8$, $b = 0.9$. Approximation (solid line) compared to simulations with $\epsilon = 10^{-3}$ (squares) and $\epsilon = 10^{-4}$ (circles).

and analogical for $\langle T_r \rangle, \langle T_r^2 \rangle$ with appropriate integration boundaries for the right branch and potentials according to Eq. (13). Equation (20) proves again the equality of current (pulse rate) and the inverse of the sum of the passage times, i.e., the mean interspike interval.

With Eqs. (20) and (21) the noise-to-signal ratio (4) can be calculated by

$$R(D) = \frac{\sqrt{\langle T_l^2 \rangle + \langle T_r^2 \rangle - \langle T_l \rangle^2 - \langle T_r \rangle^2}}{\langle T_l + T_r \rangle}. \tag{22}$$

This quantity exhibits a minimum with respect to the noise strength (Fig. 12), indicating a coherent (i.e., most regular) spike train for a particular noise level. Results of the simulations, depicted in the same figure, confirm the analytical findings, particularly the rough position of the maximum as well as its depth. It is remarkable that a finite ϵ (cf. simulations) deepens the minimum and shifts it toward larger values of D. Because there is no doubt that the coherence is destroyed from a larger value of ϵ on, there should be a critical value of ϵ for which R becomes minimal.

CONCLUSIONS

We have presented analytical and numerical results for the dynamics of a nerve cell driven by white noise. In the limit of a fast voltage variable, we could calculate the stationary probability densities, the mean interspike interval, and its relative error, as well as the slope of the pulse rate with respect to a slow signal. Results are in accordance with former numerical results [6,10]. Our analytical study has revealed that the pulse rate exhibits a maximum versus the slope of the recovery-null cline and has proven the existence of a minimum of the interval error (noise-to-signal ratio). All these findings were confirmed by numerical simulations of the full system.

ACKNOWLEDGMENTS

This work was supported by Deutsche Forschungsgemeinschaft: Graduiertenkolleg 268 ''Dynamik und Evolution zellulärer und makromolekularer Prozesse'' (B.L.) and Sfb 555 ''Komplexe nichtlineare Prozesse'' (L.S.-G.).

[1] R.A. FitzHugh, Biophys. J. **1**, 445 (1961).
[2] A.C. Scott, Rev. Mod. Phys. **47**, 487 (1975).
[3] A. Longtin, J. Stat. Phys. **70**, 309 (1993); A. Longtin, Nuovo Cimento D **17**, 835 (1995).
[4] J.J. Collins, C.C. Chow, and T.T. Imhoff, Phys. Rev. E **52**, 3321 (1995).
[5] X. Pei, K. Bachmann, and F. Moss, Phys. Lett. A **206**, 61 (1995).
[6] D.R. Chialvo, A. Longtin, and J. Müller-Gerking, Phys. Rev. E **55**, 1798 (1997).
[7] A. Longtin and D.R. Chialvo, Phys. Rev. Lett. **81**, 4012 (1998).
[8] A. Neiman, L. Schimansky-Geier, F. Moss, B. Shulgin, and J.J. Collins, Phys. Rev. E **60**, 284 (1999).
[9] J.B. Baltanas and J.M. Casado, Physica D **122**, 231 (1998).
[10] A. Pikovsky and J. Kurths, Phys. Rev. Lett. **78**, 775 (1997).
[11] J.M. Casado, Phys. Lett. A **235**, 489 (1997).
[12] S.R. Massanés and C.J.P. Vicente, Phys. Rev. E **59**, 4490 (1999).
[13] D.E. Postnov, S.K. Han, T.Y. Yim, and O.V. Sosnovtseva, Phys. Rev. E **59**, 3791 (1999).
[14] Ch. Kurrer and K. Schulten, Phys. Rev. E **51**, 6213 (1995).
[15] H. Hempel, L. Schimansky-Geier, and J. García-Ojalvo, Phys. Rev. Lett. **82**, 3713 (1999).
[16] A. Neiman, L. Schimansky-Geier, A. Cornell-Bell, and F. Moss, Phys. Rev. Lett. (to be published).
[17] R. Graham and H. Haken, Z. Phys. **243**, 289 (1971).
[18] G.G. Izus, R.R. Deza, and H.S. Wio, Phys. Rev. E **58**, 93 (1998).
[19] T. Alarcon, A. Perez-Madrid, and J.M. Rubi, Phys. Rev. E **57**, 4879 (1998).
[20] V.I. Melnikov, Phys. Rev. E **48**, 2481 (1993).
[21] The constants are $x_\pm = \pm 1/\sqrt{3}, y_\pm = \pm 2/(3\sqrt{3})$.
[22] W. Ebeling, H. Herzel, W. Richert, and L. Schimansky-Geier, Z. Angew. Math. Mech. **66**, 141 (1986).
[23] For $y > y_+$ or $y < y_-$, cos and arccos have to be replaced by cosh and arccosh in the inverse function for the right and left branch, respectively.
[24] B. McNamara and K. Wiesenfeld, Phys. Rev. A **39**, 4854 (1989).
[25] H.A. Kramers, Physica (Amsterdam) **7**, 284 (1940).
[26] C. W. Gardiner, *Handbook of Stochastic Methods* (Springer, Berlin, 1983).